

Description and quantification of pteropod shell dissolution:

A sensitive bioindicator of ocean acidification

Nina Bednaršek^{1,2,3,*}, Geraint A Tarling¹, Dorothee CE Bakker², Sophie Fielding¹, Anne Cohen⁴, Alan Kuzirian⁵, Dan McCorkle⁴, Bertrand Lézé², Roberto Montagna²

¹ British Antarctic Survey, High Cross, Madingley Rd, Cambridge, CB3 0ET, UK

² School of Environmental Sciences, University of East Anglia Research Park, Norwich, NR4 7TJ UK

³ University of Nova Gorica, Laboratory for Environmental Research, Vipavska 13, Rožna Dolina, 5000 Nova Gorica, Slovenia

⁴ Woods Hole Oceanographic Institution, Department of Geology and Geophysics, 266 Woods Hole Rd, Woods Hole, MA 02543

⁵ Marine Biological Laboratory, 7 MBL Street, Woods Hole, Woods Hole, MA 02543

Please note that this is a copy of the author's accepted manuscript of the paper. Minor changes may have been made to the text and certain details of the figures during the proof stage.

This document is stored on the NERC Open Research Archive at <http://nora.nerc.ac.uk/500554/> and a copy of the final published article can be found at <http://dx.doi.org/10.1111/j.1365-2486.2012.02668.x>

Description and quantification of pteropod shell dissolution:

A sensitive bioindicator of ocean acidification

1 Nina Bednaršek^{1,2,3, *}, Geraint A Tarling¹, Dorothee CE Bakker², Sophie Fielding¹, Anne
2 Cohen⁴, Alan Kuzirian⁵, Dan McCorkle⁴, Bertrand Lézé², Roberto Montagna²

3 ¹ British Antarctic Survey, High Cross, Madingley Rd, Cambridge, CB3 0ET, UK

4 ² School of Environmental Sciences, University of East Anglia Research Park, Norwich, NR4
5 7TJ UK

6 ³ University of Nova Gorica, Laboratory for Environmental Research, Vipavska 13, Rožna
7 Dolina, 5000 Nova Gorica, Slovenia

8 ⁴ Woods Hole Oceanographic Institution, Department of Geology and Geophysics, 266 Woods
9 Hole Rd, Woods Hole, MA 02543

10 ⁵ Marine Biological Laboratory, 7 MBL Street, Woods Hole, Woods Hole, MA 02543

11
12
13 *Corresponding author: nina.bednarsek@ung.si, Tel: +386 (0)53315204, Fax: +386
14 (0)53315296

15
16 Keywords: pteropods; ocean acidification; aragonite shell; shell dissolution; dissolution
17 quantification; bioindicator.

19 *Abstract*

20 Anthropogenic ocean acidification is likely to have negative effects on marine calcifying
21 organisms, such as shelled pteropods, by promoting dissolution of aragonite shells. Study of
22 shell dissolution requires an accurate and sensitive method for assessing shell damage. Shell
23 dissolution was induced through incubations in CO₂ enriched seawater for between 4 and 14
24 days. We describe a procedure that allows the level of dissolution to be assessed and classified
25 into three main types: Type I with partial dissolution of the prismatic layer; Type II with
26 exposure of underlying crossed-lamellar layer, and Type III, where crossed-lamellar layer
27 shows signs of dissolution. Levels of dissolution showed a good correspondence to the
28 incubation conditions, with the most severe damage found in specimens held for 14 d in
29 undersaturated condition ($\Omega \sim 0.8$). This methodology enables the response of small pelagic
30 calcifiers to acidified conditions to be detected at an early stage, thus making pteropods a
31 valuable bioindicator of future ocean acidification.

33 ***Introduction***

34 Modelling the ocean-carbon cycle under the 'business-as-usual' IS92a scenario, aragonite
35 undersaturation is predicted for the Southern Ocean surface waters by 2100 as a result of
36 anthropogenic ocean acidification (Caldeira and Wickett 2003; Orr et al. 2005) and possibly
37 sooner in wintertime (McNeil and Matear 2008). Pteropods are likely to be the first indicators
38 of where ocean acidification is starting to impact high-latitude pelagic marine communities
39 since they are one of the few pelagic organisms to make their shells entirely out aragonite, a
40 relatively soluble form of calcium carbonate (Orr et al. 2005; Fabry et al.2008).

41 Ocean acidification, and the modifications it induces to carbonate chemistry, will impact the
42 shells of pelagic calcifiers in two ways. Firstly, it will alter the ability of the organism to calcify
43 and secondly, it will dissolve the calcified shell. In terms of calcification, Comeau et al. (2010)
44 found that a decrease in saturation of aragonite in seawater (Ω) decreased the level of
45 calcification in pteropod shells (*Limacina helicina*) significantly, although some calcification
46 still occurred at relatively low levels of saturation. From these results, Comeau et al. (2011)
47 predicted that *Limacina helicina* will become unable to precipitate CaCO_3 over much of the
48 Arctic by the end of the century under the IPCC SRES A2 scenario. Also, such predictions do
49 not take into account the effect of aragonite undersaturation on shell dissolution, which may act
50 to accelerate the vulnerability of pelagic calcifiers. For instance, in a pilot study, Orr et al.
51 (2005) noted significant corrosion to the shells of the pteropod *Clio pyramidata* incubated in
52 water undersaturated for aragonite for 48 h.

53 Shell dissolution has been used as a useful indicator of aragonite undersaturation horizon ($\Omega < 1$)
54 in sedimentary studies. For example, Ruddiman & Heezen (1967) determined the percentage of
55 the non-carbonate versus carbonate material to assess dissolution. Almogi-Labin et al. (1986)
56 examined changes on the surface of pteropods shells using light microscopy and categorised

57 them into stages, from transparent, indicating an excellent state of preservation, to
58 opaque/white, indicating corrosion. Opacity under light microscopes was also adopted as an
59 index of aragonite dissolution by Haddad & Droxler (1996), Gerhardt et al. (2000), Gerhardt &
60 Henrich (2001), and Manno et al. (2006).

61 Each of the above methods was developed to assess effects on mainly dead organisms below
62 the saturation horizon where levels of dissolution are substantial. However, the effects of
63 modern-day ocean acidification are likely to be small and sub-lethal, probably involving minute
64 changes to the shell-surface. In such instances, light microscopy may not show sufficient
65 details to detect such changes and there is a need for more precise and sensitive assessment
66 methods. Scanning electron microscopy (SEM) can provide the extra resolution required to
67 carry out such assessments. Nevertheless, the vacuum environment of SEM may otherwise
68 introduce artefacts unless appropriate preparation techniques are used. A particular hazard in
69 studying shell microstructure with SEM is the fragility of the thin pteropod shell walls (Bé et
70 al. 1972). In the *Limacinadae* family, this microstructure consists of underlying thick cross-
71 lamellar layers and an upper thin prismatic layer that is covered with an organic layer
72 (periostracum; Fig. 1). It is particularly thin in juveniles and prone to mechanical damage that
73 may contribute to errors in interpreting damage induced by dissolution. Furthermore, the
74 periostracum must be removed before SEM analysis, as remnants of this layer prevent an
75 accurate examination of the shell surface, or be misinterpreted as shell damage.

76 This article describes a method for preparing pteropod shells and analysing dissolution on them
77 that is capable of fine resolution and sensitive to the fragility of the specimens. We show that
78 the technique can reveal the processes involved in the dissolution of pteropod shells under
79 acidified conditions. We further develop a standardized metric scheme with which to categorise
80 different levels of dissolution damage. This scheme establishes a benchmark against which the
81 dissolution status of different pteropod species and populations can be compared. Such
82 information is essential for an informed debate on the threat to shelled pteropods by ocean

83 acidification.

84

85 ***Materials and Methods***

86 Pteropod specimens were collected with slowly-hauled fine-meshed nets from various locations
87 within the Scotia Sea, Southern Ocean (see Supplementary Information). Micro- and meso-
88 zooplankton sized specimens (mainly juveniles) were collected by vertically integrating the
89 upper 200 m using a vertical Bongo (mesh size 200 μm with an opening of 0.5 m^2) and a towed
90 Bongo net (2 nets, with 300 μm and 600 μm mesh sizes). Macrozooplankton sized specimens
91 (adults) were caught in RMT8 and RMT25 trawls (mesh size 4.5 mm). All the organisms used
92 in incubations were alive at the start of the experiments, except for the natural control
93 specimens that were preserved in 70% ethanol immediately. The majority of incubations were
94 carried out on juvenile specimens for between 4 and 14 d at various Ω saturation levels.
95 Mortality at the end of the experiments was low (<10%) and dead specimens were not
96 considered further for SEM analysis. As pteropods are prone to mechanical damage, a key factor
97 when designing the incubation apparatus was to minimise physical interference. For this
98 reason, closed blacked-out systems (2 L sealed borosilicate bottles) were used in which the
99 water was enriched with CO_2 prior to incubation. Enrichment was achieved through the
100 bubbling of different air/ CO_2 mixtures (500 ppm, 750 ppm and 1200 ppm) through 0.7 μm
101 filtered sea water until the required omega saturation level was reached. Omega was assessed
102 from measurements of DIC (dissolved inorganic carbon) and total alkalinity (TA) at the start
103 and end of each incubation experiment, which lasted for 4, 8 or 14 d (see Supplementary
104 Materials). Ω values were often different between incubation start and end points (up to ± 0.17 ,
105 Table 1), so only broad categorisations of incubation conditions were possible for comparative
106 purposes, those being: a) supersaturated ($\Omega > 1.2$) b) transitional ($\Omega = 0.95$ to 1.2) and c) Ω
107 undersaturated ($\Omega < 0.95$; Table 1). The experiments with Ω supersaturated conditions lasted
108 for 8 days while transitional and Ω undersaturated experiments lasted for 14 days. The

109 incubation bottles were seeded with either live juveniles or adult *Limacina helicina antarctica*
110 or adult *Clio pyramidata* forma *antarctica*. and incubated for the set period, after which, they
111 were preserved in 70% ethanol. Specimens were also extracted directly from the nets and
112 preserved as above, so as to provide a control for incubation effects.

113 *Shell preparation for SEM analysis* (Fig. 2): Shell preparation was performed in five major
114 stages: a) removal of abiogenic crystals from the shell surface, b) dehydration, c) mounting on
115 the SEM stub, d) removal of the organic layer and e) sputter coating and SEM analysis.

116 (a) *Removing abiogenic crystals from the shell surface*: At the time of sample collection from
117 the field, pteropod samples were directly transferred from seawater to 70 % ethanol. This
118 resulted in the precipitation of various crystalline structures on the shell surface. To remove
119 crystal deposits from the shell, surface the samples were transferred from 70 % ethanol (in
120 which they were kept from the time of sample collection) to 50 % ethanol for 2-3 minutes.
121 They were subsequently transferred to distilled water (3-5 minutes). Two different procedures
122 for removing the precipitated crystals on pteropod shells were tested for their ease of use and
123 efficiency. For the first method, hydrogen peroxide (H₂O₂) was used to dissolve the crystals.
124 The hydrogen peroxide concentration and the exposure time were adjusted to maintain shell
125 integrity. Samples were treated with two consecutive rinses in 6 % H₂O₂ for 15-20 minutes.
126 Alternatively, Triton-X-100 and slight sonication was used to dislodge surface material. The
127 shells were put into 100-200 ml of 0.5 % Triton-X-100 in seawater and sonicated for 5 seconds.
128 The sonication procedure was repeated two to three times at 5 seconds each. In this study, we
129 mainly used the first approach for abiogenic crystal removal which we recommend for future
130 use. Finally, all samples were washed twice in distilled water for a total of five minutes.

131 (b) *Dehydration*: Dehydration was undertaken using 2,2-Dimethoxypropane (DMP; chemical
132 formula: (CH₃)₂C(OCH₃)₂), and 1,1,1,3,3,3-hexamethyldisilazane (HMDS; chemical formula:
133 (CH₃)₃SiNH₃Si(CH₃)₃). Before starting dehydration with DMP, the shells were transferred to 50
134 % methanol for two 5 min washes then transferred to 85 % methanol (10 minutes). Complete

135 tissue dehydration was accomplished by immersion in DMP: two changes at 15-20 minutes
136 each. It was important not to let the shells air dry at this stage, so they were transferred to a 1:1
137 mixture of DMP and HMDS for about 10 minutes, followed by 100 % HMDS for 20-25
138 minutes twice. The HMDS was subsequently allowed to evaporate allowing the shells to dry
139 completely (Fig. 2). The moderate vapour pressure and very low surface tension of HMDS
140 allowed the shells to dry without distortion or loss of shell integrity.

141 *(c) Mounting on the SEM stub:* Fine brushes were used to mount the dry shells on aluminium
142 SEM stubs using colloidal graphite. Extreme care was needed when manoeuvring the shell with
143 a brush, as this could cause structural damage or even shell collapse. Shells had to be
144 positioned in a dorso-ventral position for the oxygen plasma etching reaction (see below) to
145 expose the maximum surface area, and for qualitative examination. To examine the changes on
146 the growing edge, a proximo-distal position of the shell with the aperture on top was chosen.

147 *(d) Removal of the organic shell layer using oxygen plasma etching:* The samples had to be
148 completely dry and oriented to expose the maximum surface area prior to etching. A BIO-RAD
149 RF plasma barrel etcher PT7150 was used with a forward power of ≈ 200 Watts and a reflected
150 power of ≈ 5 Watts. The shells were typically etched for between 10-30 minutes, depending on
151 the power of the etcher.

152 Adult shells are less fragile than juvenile shells, hence less sensitive preparation procedures
153 were sufficient. For instance, for rapid removal of abiogenic crystals, it was possible to use a
154 stronger solution of hydrogen peroxide (30 % H₂O₂). This concentration was also reasonably
155 efficient at removing the periostracum, although it did not perform as well as the plasma
156 etching. Two sequential immersions in 30% H₂O₂ for 10-12 minutes each were required to
157 remove the abiogenic crystals and most of the overlying organics. Transfer to 100 % HMDS for
158 25-30 minutes was sufficient for complete dehydration and drying.

159 *Categorization scheme for pteropod shell dissolution:* Analysis of the SEM photos enabled
160 observation of the shell surface and identification of shell dissolution; notably pitting, cracks,

161 and areas where aragonite crystals were absent or porous. Different stages in the level of
162 dissolution were recognisable and so a scheme was devised that categorised these stages into
163 three types (Type I, II, III) which are described in detail in a later section.

164 *Application of scheme to incubated specimens:* The categorisation scheme above was applied in
165 a semi-quantitative manner using image segmentation analysis to assess the extent of each
166 dissolution type over the shell surface. Analyses were performed only on those pteropods that
167 were successfully maintained in the experimental conditions, therefore excluding mortality as a
168 factor of variability. Overall, 50 animals were examined; 20 animals from the natural
169 environment, 9 from the supersaturated incubations, 11 from the transitional incubations (Ω
170 ~ 1), and 11 from the undersaturated incubations. For each individual, 15-20 SEM photographs
171 were generated across the shell surface area, which amounted to a total of 750 SEM
172 micrographs, on which image the segmentation analysis was performed. This procedure is
173 described in Supplementary Materials. Statistical differences in dissolution levels between
174 incubations were determined with a Kruskal-Wallis 1-way ANOVA on ranks followed by
175 Dunn's Method to determine which pairwise differences were significantly different ($p < 0.05$).

176

177 ***Results and Discussion***

178 *Shell preparation method* The shell preparation method proved to be non-destructive, providing
179 specimens with clean and intact shell surfaces, thus limiting the occurrence of methodological
180 artefacts and rendering an intact crystalline layer suitable for further SEM examination. Each of
181 the steps is considered in further detail below:

182 *(a) Removal of abiogenic crystals and bacteria:* The transfer of samples from seawater to 70 %
183 ethanol caused rapid water removal and the precipitation of phosphate, calcium and sodium
184 chloride (NaCl) crystals on the shell surface. Without applying the shell preparation method,
185 the crystals covered much of the shell surface, and made it impossible to examine it for

186 evidence of dissolution (Fig. 3 shows various abiogenic crystals). Phosphate crystals occurred
187 in the struvite (Fig. 3a), rosette (Fig. 3b) or in triple phosphate forms (Fig. 3c). Sodium chloride
188 formed cubes (Fig. 3b). In addition, bacteria from seawater attached to the surface and in some
189 cases, completely covered the shell (Fig. 3d). Therefore, removal of abiogenic crystals with
190 H₂O₂ was necessary before SEM examination.

191 An alternative approach to minimise or avoid the precipitation of abiogenic crystals on the
192 shell surface during sample fixing would have been to place samples in a low ethanol grade
193 (50 %), followed by subsequent, transfer to higher concentrations (up to 70%) in gradual steps.
194 This method allows dilution of the salts in the high concentrations of seawater and their
195 subsequent removal. Samples should not be fixed in buffered formalin for dissolution studies,
196 because formalin dissolves aragonite crystals.

197 *(b) Removal of the organic layer:* Although extremely thin, the outer organic layer is fully
198 embedded within the surface crystals of the shell. This periostracum must be removed before
199 SEM examination for two reasons: i) microstructural changes of the aragonite crystals can
200 otherwise be obscured and ii) disintegration of organic remnants during coating for SEM can
201 lead to misinterpretation of dissolution in the subsequent analysis or obscure signs of shell
202 dissolution. Juvenile shells are especially fragile and prone to mechanical damage and
203 disintegration, thus an inappropriate method could easily damage these delicate shells. A
204 common way to etch the surface of SEM samples is acid hydrolysis that denatures surface
205 proteins and thus, eliminates the periostracum. However, acid treatment is unsuitable for shell
206 dissolution studies because it dissolves aragonite crystals. Therefore, oxygen plasma etching
207 was found to be a non-destructive and efficient procedure for removing the periostracum from
208 delicate pteropod shells.

209 *(c) Preparation artefacts:* Drying of the samples and mounting them on SEM stubs were the
210 steps with the greatest potential to cause mechanical damage to the shells. Despite taking the
211 utmost care, mechanical damage (e.g. cracks, pitting, broken growing edges) mostly originated

212 from handling while mounting the samples on SEM stubs. It was nevertheless possible to
213 distinguish this type of damage from the effects of dissolution when scrutinised under SEM. In
214 addition, in shells that were not properly dehydrated, the vacuum force during coating for SEM
215 resulted in the collapse of the organic matrix (Fig. 4a,b), and cracked and chipped growing
216 edge (Fig. 4c), and pitted surfaces (Fig. 4d). Occasional damage to shells, particularly at the
217 growing edge, occurred most frequently in juveniles that had been incubated in Ω
218 undersaturated water, where dissolution had weakened the shells. Hence it was important to dry
219 fully and remove the organic layer prior to coating. DMP and HMDS were used to avoid these
220 artefacts. DMP did not cause any deterioration or physical change to specimens (Maser &
221 Trimble 1977). HMDS dried the organic meshwork and stabilized the complex protein
222 structures of the shell without changing or destroying any structural features. This was achieved
223 by decreasing surface tensions during drying with HMDS; otherwise damage to fragile
224 structures within the shell would occur. HMDS is an inexpensive, easy to handle, and time-
225 saving alternative to critical point drying.

226 The methodology used for live juveniles was equally effective for adult *L. helicina ant.* Adults
227 were rare in our samples but were easier to work with than juveniles, since they are larger to
228 handle and their shells are more compact. This allowed certain preparation steps to be
229 modified. For example, H_2O_2 could be applied in higher concentrations and for longer
230 durations to remove the abiogenic crystal precipitation. This reduced or totally eliminated the
231 time required to remove the organic layer by oxygen plasma etching. Additionally, dehydration
232 steps could be shortened (for instance, through eliminating 85 % methanol and double
233 immersion in DMP), as long as the HMDS step was long enough to attain proper water
234 removal.

235 The method also worked effectively for *Clio pyramidata f. ant.*, despite differences in the shell
236 structure compared to *L. helicina ant.* The shell microstructure of *Clio pyramidata f. ant.* is
237 helical with a prismatic layer that is a few microns thick and covered by a thin organic layer

238 (Bé and Gilmer 1977).

239 With the organic layer removed, the crystal structure of the prismatic layer was revealed (Fig.
240 4e). For samples exposed to high CO₂ levels, SEM observations revealed initial (Type I; Fig.
241 5), intermediate (Type II; Fig. 6) and advanced (Type III: Fig. 7) dissolution levels on the shell.

242
243 *The process of dissolution and categorization scheme for shell dissolution* Dissolution of the
244 aragonite crystals on the shell surface and growing edge was assessed by comparing SEM
245 images of pteropods exposed to high CO₂ levels with those of controls. The progression of shell
246 dissolution was divided into four stages based on the level of shell damage: No dissolution, and
247 Type I, II and III (Table 2). A pteropod shell taken from ambient seawater with supersaturated
248 conditions for omega typically had a smooth, sleek shell surface (Fig. 4e) and the shell
249 structure was compact with very little intracrystalline porosity. Type I dissolution corresponded
250 to a mild degree of dissolution defined by small effects on the upper prismatic layer and initial
251 exposure of aragonite crystals. As a result of dissolution, intact heads of the aragonite crystals
252 appeared as 'cauliflower heads' (Fig. 5a,b). There were only rare deep intrusions into the
253 crossed-lamellar layer but the shell had become porous, less compact, and hence more fragile
254 than an intact shell.

255 The next level of dissolution was categorised as Type II dissolution. It was represented by the
256 partial disappearance of the prismatic layer. The crossed-lamellar layer had been exposed, but
257 not affected by dissolution (Fig. 6b). Progressive roughening of the shell surface induced by
258 dissolution substantially enhanced the rate of shell dissolution, as first suggested by Acker &
259 Byrne (1989). Shell porosity had increased, and the shell surface had numerous, large damaged
260 patches across the shell surface (Fig. 6a).

261 As the dissolution process continued, an extended degree of porosity and dissolution of the
262 crossed-lamellar layer was evident over the shell surface (Fig. 7b). In the case of Type III
263 dissolution, the crystals of the crossed-lamellar layer had been partly eroded and became

264 thicker and chunkier in appearance (Fig. 7c). Since shell dissolution was extensive with a
265 loosely organised crystal structure, shell integrity had been lost and the shell was prone to
266 fragmentation and increased frailness (Fig. 7a).

267
268 *Dissolution at the growing edges* The dissolution categorization scheme for the shell surface
269 was also applicable to the growing edge. At the onset of dissolution, the intact crystal structure
270 (Fig. 8a) was replaced by 'cauliflower heads' indicating Type I dissolution (Fig. 8c). In the most
271 severe cases, dissolution transformed the crystals from long aragonite rods present on an intact
272 shell (Fig. 8b) to thick, short, loosely arranged crystals with eroded lateral edges of Type III
273 dissolution (Fig. 8d). As a result, the growing edge had become less rigid and more fragile.

274
275 *Semi-quantification of shell surface dissolution* Image segmentation allowed the extent of the
276 three different categories of shell dissolution to be estimated in a semi-quantitative manner.

277 There were statistically significant differences in dissolution levels between natural and
278 incubated specimens and also between different incubations treatments (Kruskall-Wallis 1-way
279 ANOVA on Ranks, $H = 29.15$ to 35.38 , $P < 0.001$; Fig 9). After incubation in supersaturated
280 conditions ($\Omega \sim 1.65$) for 8 days, roughly half of the shell surface was covered with Type I
281 dissolution (Fig. 9a). Given that very little dissolution was observed in natural field samples
282 extracted from supersaturated ambient conditions, we considered such dissolution to be an
283 incubation effect and used as a baseline with which to compare against other incubations.

284 Type I dissolution was also present on shells incubated in transitional conditions for 14 days
285 but covered 80% of the surface area of each shell (SD=15) with a remaining 15% (SD=10)
286 covered with Type II dissolution. In shells incubated in undersaturated conditions for 4 d, Type
287 II dissolution covered 26% of the shell (SD=6; Fig. 10) and there was evidence of Type III
288 dissolution, although only over 3% of the shell surface (SD= 3). In specimens incubated for 14
289 d in undersaturated conditions, Type III dissolution was present across one third of the total

290 shell surface (31% coverage, SD=6; Fig. 9a). The type and extent of dissolution was consistent
291 across pteropods incubated in similar conditions as evidenced by the low standard deviations
292 (Fig. 9a).

293 The fact that Type I dissolution occurred when the organism was held in supersaturated
294 conditions for 8 days and the organic layer was intact raises questions about the role of the
295 organic layer as a protection against dissolution. Clark and George (1999) postulated that the
296 organic layer would have to be severely altered or destroyed before the crystal structure of the
297 shell would be affected by chemicals, i.e. acidic attack. Similarly, Vermeij (1987) regarded a
298 thick periostracum as a molluscan adaptation for slowing down dissolution. A microstructure
299 with a high organic content provides high resistance to dissolution by shrouding the crystals
300 (Harper 2000). However, while Glover & Kidwell (1993) regarded the organic layer as a
301 protection against dissolution, they also acknowledged the possibility that the organic layer
302 could enhance dissolution by promoting growth of acid-releasing microbes. We propose that
303 the periostracum does not provide protection from acidified waters.

304 Altogether, the development of a reliable method by which to prepare pteropod shells for SEM
305 analysis has allowed us to describe in detail the process of how shell-surface dissolution
306 progresses from its initial stages to severe levels of damage. It has also allowed us to develop
307 an easily applicable categorization scheme for types of shell dissolution and subsequently, a
308 means of obtaining a semi-quantitative assessment of the extent of different types of dissolution
309 on pteropod shells, with the assistance of some custom-made freeware for image segmentation
310 analysis (see Supplementary Materials). With appropriate calibration, these developments will
311 in turn allow levels of dissolution to be quantified and contribute to studies of oceanic carbon
312 budgets. Establishing functional responses between aragonite saturation state and the extent of
313 dissolution in pteropod shells is the next important step in this process. Such functions are an
314 important aspect of not only considering the biogeochemical consequences of the dissolution of
315 calcifiers but also their future viability in acidifying oceans. Based on their demonstrated

316 response to subtle changes in carbonate chemistry, this study suggests that the monitoring of
317 pteropod shell dissolution can serve not only as a proxy of saturation state in the past (Gerhardt
318 & Henrich 2001), but also as a sensitive bioindicator of modern day ocean acidification. Wider
319 application will also increase our ability to assess the impact of these changes on other pelagic
320 calcifiers.

321

322 *Acknowledgements*

323 Thanks go to the officers and crew of the RRS James Clark Ross for their support during the
324 cruise JR177, from which the live material was obtained and experiments were conducted . NB
325 was supported by the FAASIS (Fellowships in Antarctic Air-Sea-Ice Science), a Marie Curie
326 Early Stage Training Network with grant number MEST-CT-2004-514159. GT and SF carried
327 out this work as part of the DISCOVERY 2010 and ECOSYSTEM programmes at BAS.

328

329

330

331

332

333

334

335

336

337

338

339

340

341 ***References***

342 Acker JG. and Byrne RH (1989) The influence of surface state and saturation state on the
343 dissolution kinetics of biogenic aragonite in seawater. *American Journal of Science*, 289, **9**,
344 1098-1116.

345 Almogi-Labin A, Luz B, Duplessy DC (1986) Quaternary paleo-oceanography, pteropod
346 preservation and stable-isotope record of the Red Sea. *Palaeogeography, Palaeoclimatology,*
347 *Palaeoecology*, **52**, 2-4, 195-211.

348 Bé AWH, Gilmer RW (1977) A zoogeographic and taxonomic review of euthecosomatous
349 Pteropoda. In: *Oceanic Micropalaeontology I*. (eds Ramsay ATS), pp 733-808. Academic Press
350 London.

351 Bé AWH, MacClintock C, Currie DC (1972) Helical shell structure and growth of the pteropod
352 *Cuvierina columnella* (Rang) (Mollusca, Gastropoda). *Biomineralization Research Reports*, **4**,
353 47-

354 79.

355 Berner RA and Morse JW (1974) Dissolution kinetics of calcium carbonate in sea water; IV:
356 Theory
357 of calcite dissolution. *American Journal of Science*, **274**, 108-134.

358 Byrne RH, Acker JG, Betzer PR et al. (1984) Water column dissolution of aragonite in the
359 Pacific Ocean. *Nature*, **312**, 321-326.

360 Caldeira K, Wickett ME (2003). Anthropogenic carbon and ocean pH. *Nature*, **437**, 681-686.

361 Christoudias CM, Georgescu B, Meer P (2002) Synergism in low-level vision. 16th
362 *International Conference on Pattern Recognition*, **4**, 150–155.

363 Clark GR II (1999) Organic matrix taphonomy in some molluscan shell microstructures.
364 *Palaeogeography, Palaeoclimatology, Palaeoecology*, **149**, 1-4, 305-312.

365 Comaniciu D, Meer P (2003). "Mean shift: A robust approach toward feature space analysis."
366 *IEEE Transactions on pattern analysis and machine intelligence*, 24, 5, 603-619.

367 Comeau S, Gattuso JP, Nisumaa AM et al. (2011) Impact of aragonite saturation state changes
368 on
369 migratory pteropods. *Proceedings of the Royal Society B Biological Sciences*, doi
370 0.1098/rspb.2011.0910.

371 Comeau S, Jeffree R, Teyssie JL et al. (2010) Response of the Arctic pteropod *Limacina*
372 *helicina* to projected future environmental conditions. *PLoS One* **5**, 6, e11362.

373 Dickson, AG (1981) An exact definition of total alkalinity and a procedure for the estimation of
374 alkalinity and total inorganic carbon from titration data. *Deep-Sea Research Part I.*
375 *Oceanographic Research Papers*, **28**, 609-623.

376 Dickson AG, Millero FJ (1987) A comparison of the equilibrium constants for the dissociation
377 of carbonic acid in seawater media. *Deep-Sea Research Part I. Oceanographic Research*
378 *Papers*, **34**, 1733-1743.

379 Dickson AG, Sabine CL, Christian JR (2007) Guide to best practices for ocean CO₂
380 measurements. *PICES Special Publication*, **3**, 1-191.

381 Fabry, VJ, Seibel BA, Feely RA et al. (2008) Impacts of ocean acidification on marine fauna
382 and ecosystem processes. *ICES Journal of Marine Science*, **65**, 3, 414-432.

383 Gehlen M, Bassinot FC, Chou L et al. (2005) Reassessing the dissolution of marine carbonates:
384 I. Solubility. *Deep Sea Research Part I. Oceanographic Research Papers*, **52**, 8, 1445-1460.

385 Gerhardt S, Groth H, Rühlemann C et al. (2000) Aragonite preservation in late Quaternary
386 sediment cores on the Brazilian Continental Slope: implications for intermediate water
387 circulation. *International Journal of Earth Sciences*, **88**, 4, 607-618.

388 Gerhardt S, Henrich R (2001). Shell preservation of *Limacina inflata* (Pteropoda) in surface

389 sediments from the Central and South Atlantic Ocean: a new proxy to determine the aragonite
390 saturation state of water masses. *Deep Sea Research Part I. Oceanographic Research Papers*
391 **48**, 9, 2051-2071.

392 Georgescu CM (2002) Synergism in low level vision, *16th International Conference on Pattern*
393 *Recognition, Proceedings*, **4**, 150-155.

394 Glover CP, Kidwell SM (1993) Influence of organic matrix on the post-mortem destruction of
395 molluscan shells. *The Journal of Geology*, **101**, 6, 729-747.

396 Haddad GA, Droxler AW (1996) Metastable CaCO₃ dissolution at intermediate water depths of
397 the Caribbean and western North Atlantic: Implications for intermediate water circulation
398 during the past 200,000 years. *Paleoceanography*, **11**, 6, 701-716.

399 Harper EM (2000) Are calcitic layers an effective adaptation against shell dissolution in the
400 Bivalvia? *Journal of Zoology*, **251**, 02, 179-186.

401 <http://coewww.rutgers.edu/riul/resaearch/code/EDISON/index.html>, Center for Advanced
402 Information Processing of Rutgers University, 2002.

403 Johnson KM, Sieburth JM, Williams PJJ, Brandstrom L (1987) Coulometric total carbon
404 dioxide analysis for marine studies - automation and calibration. *Marine Chemistry*, **21**, 117-
405 133.

406 Keir RS (1980) The dissolution kinetics of biogenic calcium carbonates in seawater.
407 *Geochimica et Cosmochimica Acta*, **44**, 2, 241-252.

408 Lewis E, Wallace DWR (1998) CO2SYS-Program developed for the CO₂ system calculations,
409 *Report ORNL/CDIAC-105*. Carbon Dioxide Information Analysis Center, Oak Ridge National
410 Laboratory, U.S. Department of Energy, Oak Ridge, Tennessee.

411 Maser MD, Trimble JJ (1977) Rapid chemical dehydration of biologic samples for scanning
412 electron microscopy using 2, 2-dimethoxypropane. *Journal of Histochemistry and*
413 *Cytochemistry*, **25**, 4, 247-251.

414 Manno C, Sandrini S, Tositti L et al. (2006) First stages of degradation of *Limacina helicina*

415 shells observed above the aragonite chemical lysocline in Terra Nova Bay (Antarctica). *Journal*
416 *of Marine Systems* **68**, 91-102.

417 McNeil BI, Matear RJ (2008) Southern Ocean acidification: A tipping point at 450-ppm
418 atmospheric CO₂. *Proceedings of the National Academy of Sciences* **105**, 48, 18860-18864.

419 Meer P, Georgescu B (2001) Edge detection with embedded confidence. *IEEE Transactions on*
420 *Pattern Analysis and Machine Intelligence*, **23**, 12, 1351-1365.

421 Mehrbach C, Culbertson CH, Hawley JE et al. (1973) Measurement of the apparent dissociation
422 constants of carbonic acid in seawater at atmospheric pressure. *Limnology and Oceanography*,
423 **18**, 897-907.

424 Morse JW, De Kanel J, Harris K (1979) Dissolution kinetics of calcium carbonate in seawater;
425 VII: The dissolution kinetics of synthetic aragonite and pteropod tests. *American Journal of*
426 *Science*, **279**, 5, 488-502.

427 Orr JC, Fabry VJ, Aumont O et al. (2005) Anthropogenic ocean acidification over the twenty-
428 first
429 century and its impact on calcifying organisms. *Nature*, **437**, 7059, 681-686.

430 Ruddiman WF, Heezen BC (1967) Differential solution of planktonic foraminifera. *Deep Sea*
431 *Research and Oceanographic Abstract*, **14**, 6, 801-808.

432 Seibel BA, Dierssen HM (2003) Cascading trophic impacts of reduced biomass in the Ross
433 Sea, Antarctica: Just the tip of the iceberg? *The Biological Bulletin*, **205**, 2, 93-97.

434 Vermeij, G. J. (1993) The Economics and Construction of Maintenance. In: *A natural history of*
435 *shells*, pp 39-54. Princeton University Press, Princeton, NJ.

436 Wiebe PH, Morton AW et al. (1985) New development in the MOCNESS, an apparatus for
437 sampling zooplankton and micronekton. *Marine Biology*, **87**, 3, 313-323.

438

439

440

441

442

443
444

445

446

447

448 **Figure captions**

449 Figure 1: SEM image illustrating the microstructure of the shelled pteropod *Limacina helicina*
450 *ant.* An organic layer covers a prismatic layer and an underlying crossed-lamellar crystal layer.

451

452 Figure 2: Method for the shell preparation of juvenile *Limacina helicina antarctica* stored in
453 70% ethanol.

454

455 Figure 3: Abiogenic precipitation and contamination with bacteria on the shell surface of
456 juvenile and adult pteropods. a) phosphate crystals in the struvite form (crystal rods) and NaCl
457 salts (squares); b) phosphate crystals in rosette form; c) triple phosphate crystals; d) bacterial
458 contamination with phosphate crystals in rosette form.

459

460 Figure 4: Artefacts on shells of juvenile pteropods caused by inadequate shell preparation: a, b)
461 a partly collapsed organic matrix; c) crushed and chipped growing edges generated by
462 mechanical damage or high vacuum exposure; d) pitted surfaces not caused by dissolution; e)
463 the correct shell preparation method leaves the shell and growing edge intact and, with the
464 organic layer removed, the crystal structure is revealed.

465

466 Figure 5: Type I dissolution: Aragonite crystals are missing and ‘cauliflower heads’ have
467 appeared (encircled) (Fig. 5a), the porosity has increased (Fig. 5b).

468

469 Figure 6: Type II dissolution: Larger areas of the shell surface are covered by dissolved patches,

470 where dissolution is protruding deeper (Fig. 6a), affecting the prismatic (P) layer, and exposing
471 the crossed-lamellar (CL) layer (Fig. 6b).

472
473 Figure 7: Type III dissolution: Increased shell frailness (Fig. 7a) as a result of much of the shell
474 surface being affected by dissolution (Fig. 7b), with extensive Type III dissolution causing
475 large gaps in the prismatic layer and exposing the crossed-lamellar layer (Fig. 7c).

476
477 Figure 8: The growing edge of juvenile pteropods: a) intact growing edge covered by the
478 organic layer; b) intact crystals within crossed-lamellar layer of the growing edge; c) Type I
479 dissolution - increased porosity and appearance of 'cauliflower heads' in the prismatic layer; d)
480 Type III dissolution - aragonite crystals in the crossed-lamellar layer are thicker and shorter as a
481 result of dissolution.

482
483 Figure 9: Bar graph: Correspondence between the extent of dissolution and the Ω saturation
484 state within incubations showing mean (SD) levels of dissolution according to environmental
485 conditions (natural or incubated at different levels of Ω saturation). Matrix: dissolution types
486 showing significant pairwise differences between treatments. 'x' denotes that no significant
487 differences were found; '0-diss.' denotes no detectable dissolution.

Table 1: Conditions of incubations to which live juvenile pteropods were exposed (Ω supersaturation, N=9; near-saturation, N=11 and Ω undersaturation for 4- and 14 days; N=11). Incubations were done in parallels. The value depict the mid-point between the values measured at the start and end of the incubation (\pm values depict the difference between the start and end measurements). Carbon chemistry parameters derived using Matlab CO2sys, total pH scale, Mehrbach refit by Dickson and Millero.

Experiment	Salinity	Phosphate ($\mu\text{mol/kg}$)	Silicate ($\mu\text{mol/kg}$)	Temp (deg C)	TA ($\mu\text{mol/kg}$)	DIC ($\mu\text{mol/kg}$)	pH_T	CALCULATED PARAMETERS			Ω
								($p\text{CO}_2$ (μatm))	HCO_3^- ($\mu\text{mol/kg}$)	CO_3^{2-} ($\mu\text{mol/kg}$)	
Natural control	33.86	1.33	12.5	2.9	2290.6 \pm 3.7	2123.0 \pm 61.9	8.13 \pm 0.13	318 \pm 111	1983.1 \pm 91.9	121.6 \pm 39.6	1.82 \pm 0.60
Supersaturation (experimental control) (8 days)	33.83	1.71	8.0	4.0	2360.3 \pm 3.4	2211.5 \pm 12.7	8.07 \pm 0.03	387 \pm 24	2077.8 \pm 16.60	112.7 \pm 5.4	1.70 \pm 0.08
Near-saturation	33.83	1.80	12.5	4.0	2316.8 \pm 1.3	2245.0 \pm 14.9	7.83 \pm 0.05	690 \pm 75	2144.7 \pm 17.1	67.9 \pm 6.3	1.03 \pm 0.09
Undersaturation (4 days)	33.82	1.15	10.1	4.0	2323.1 \pm 8.9	2295.5 \pm 5.4	7.70 \pm 0.01	940 \pm 27	2192.7 \pm 5.0	51.6 \pm 1.8	0.78 \pm 0.03
Undersaturation (14 days)	33.83	1.80	12.5	4.0	2330.3 \pm 6.4	2298.3 \pm 0.0	7.73 \pm 0.01	883 \pm 12	2191.0 \pm 4.4	54.8 \pm 0.90	0.83 \pm 0.02

Table 2: Summary of the main features of each dissolution type

Dissolution type	Description	Ω value when first observed
Type I	<ul style="list-style-type: none"> • First indices of slightly increased porosity • Aragonite crystals within upper-prismatic layer affected by dissolution with ‘cauliflower heads’ present 	<ul style="list-style-type: none"> • In small extent present in natural environment • Widespread at decreased Ω supersaturated state
Type II	<ul style="list-style-type: none"> • Increased porosity • Damage patches more extensive and numerous • Prismatic layer partially/completely dissolved, crossed-lamellar layer exposed 	<ul style="list-style-type: none"> • In small extent at Near-saturation Ω state with (transition between Ω super- and undersaturation occurs) • In larger extent in undersaturated conditions
Type III	<ul style="list-style-type: none"> • Damage extent and porosity resulting in less compact crystal structure • Compromised shell integrity and extreme frailness • Dissolution within crossed-lamellar layer with crystals thicker and chunkier 	<ul style="list-style-type: none"> • At near-saturated Ω conditions • Larger, more extensive patches in the Ω undersaturated ($\Omega \sim 0.8$) and progressing with the time of exposure

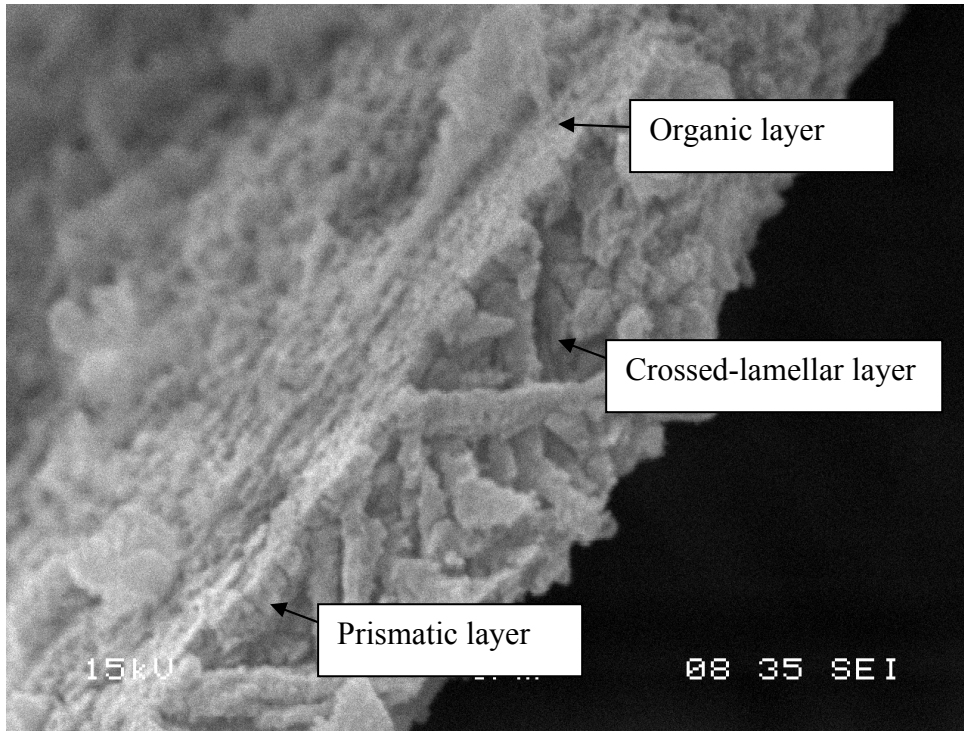


Figure 1:

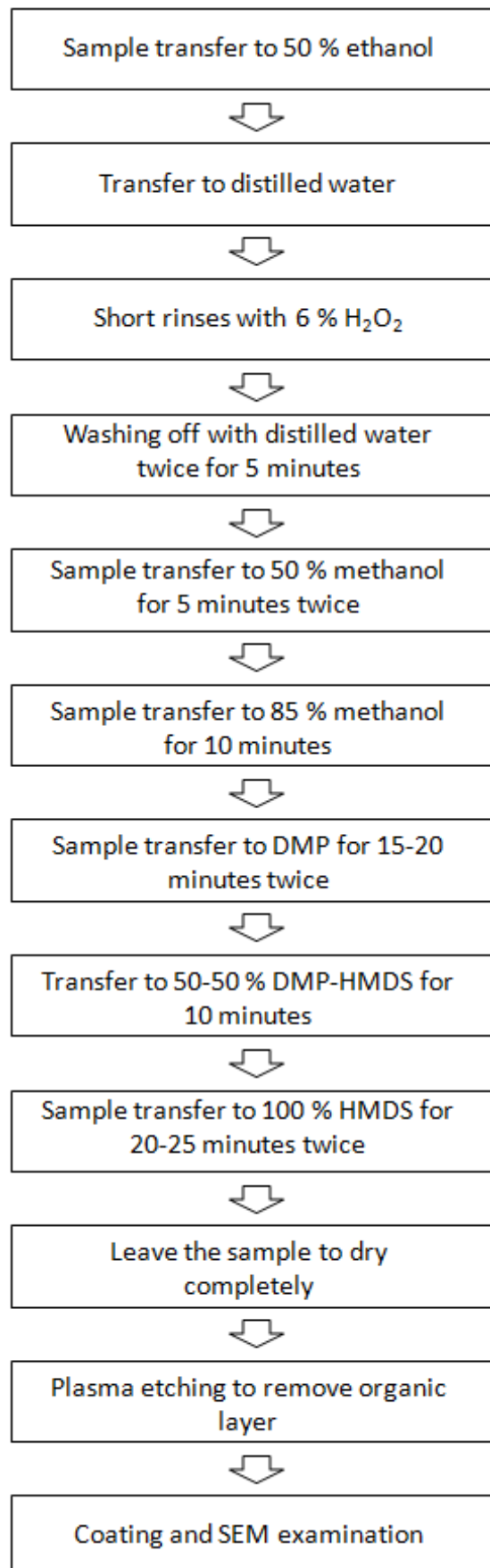


Figure 2:

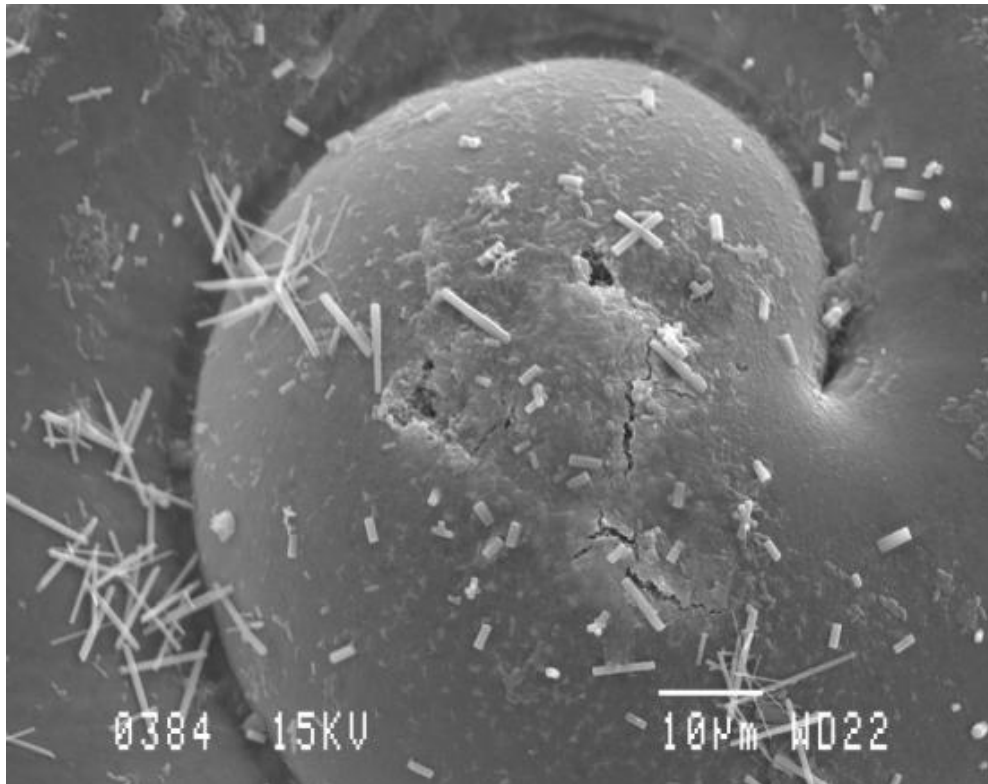


Figure 3a:

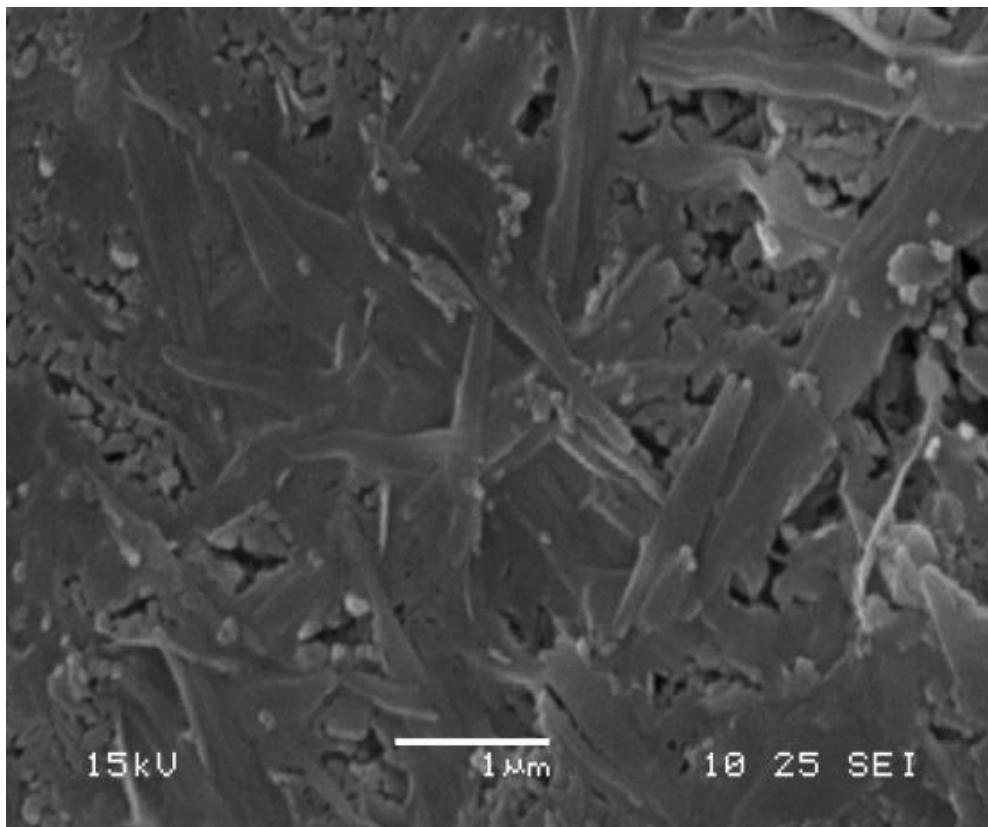


Figure 3b

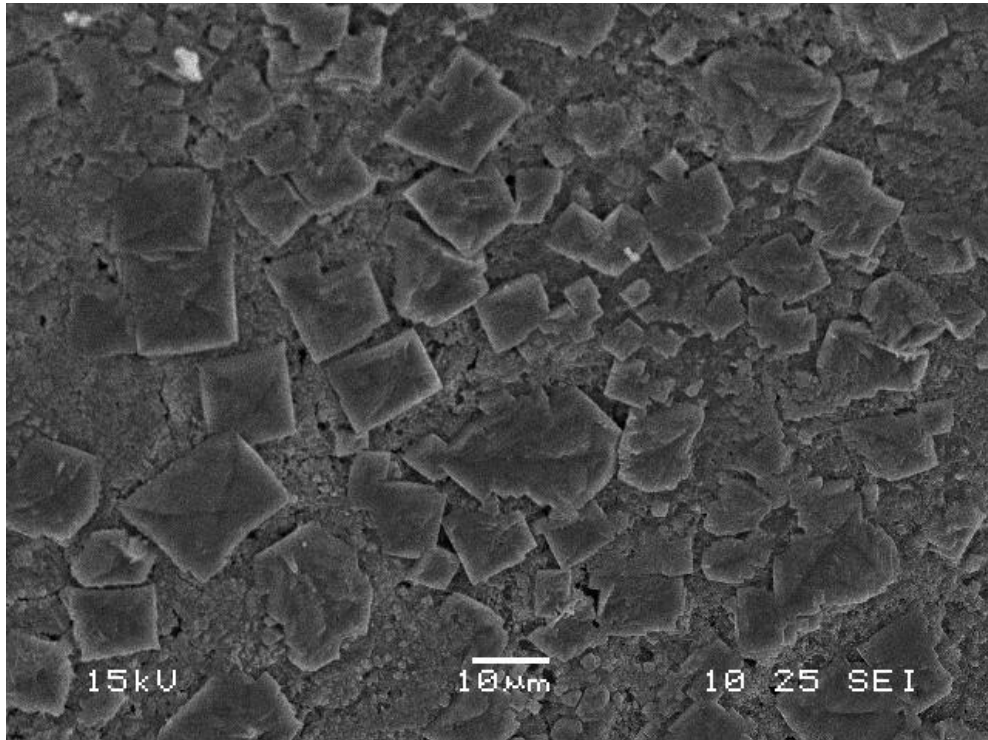


Figure 3c:

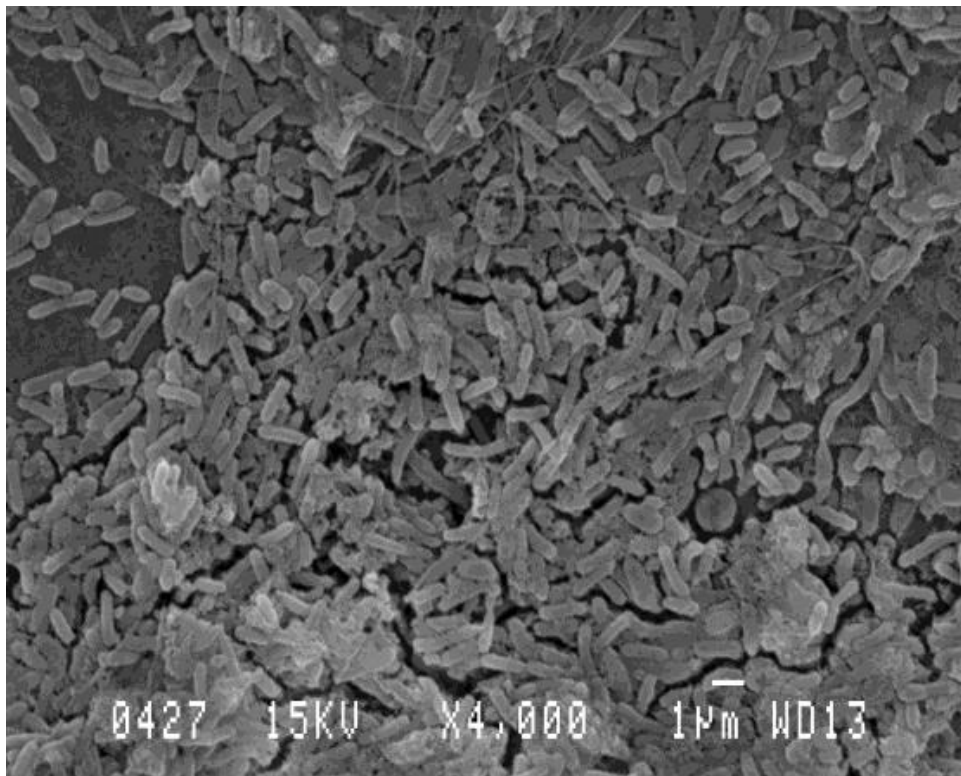


Figure 3d:

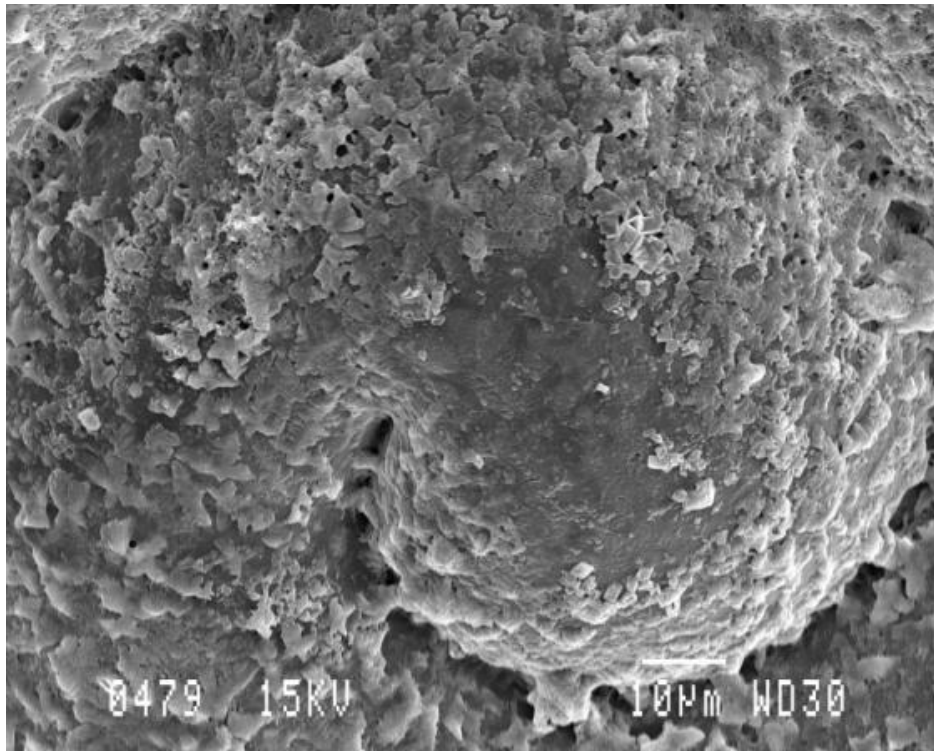


Figure 4a:

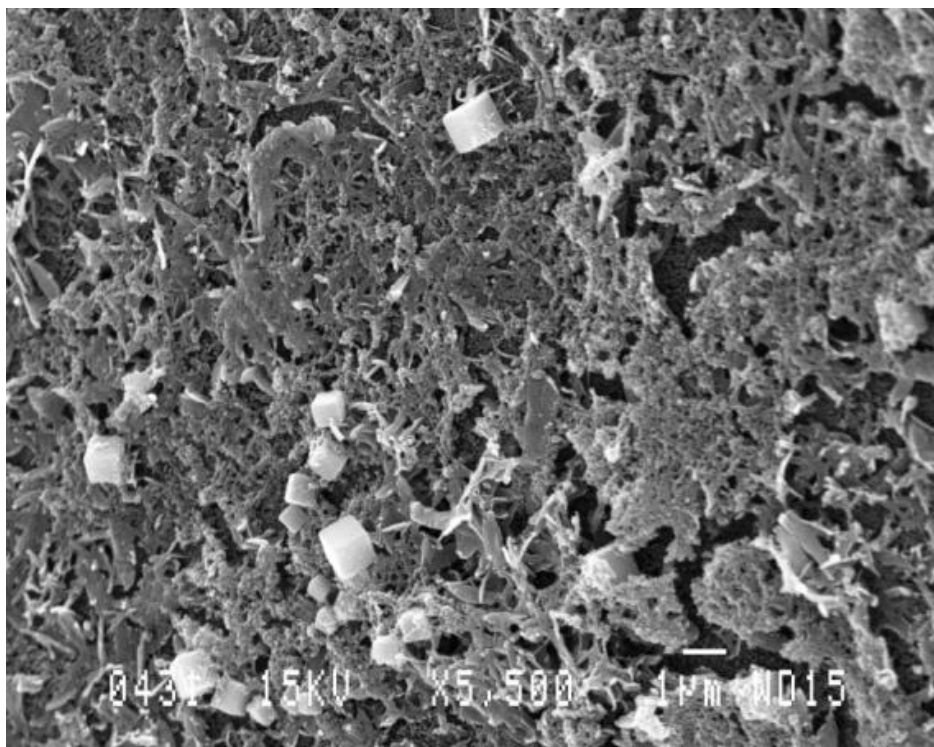


Figure 4b:

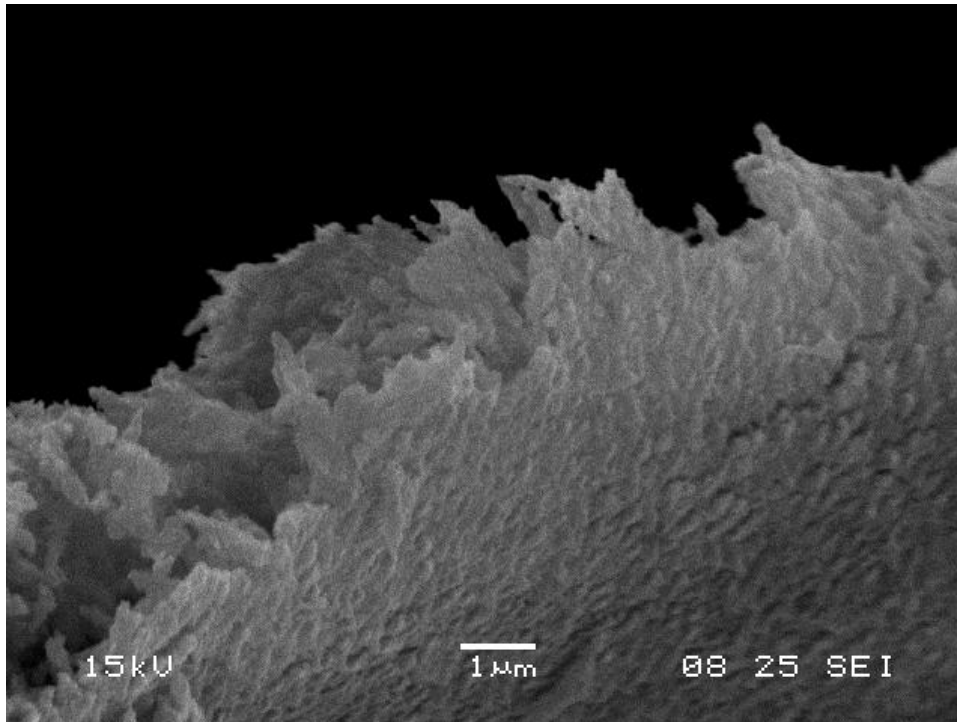


Figure 4c:

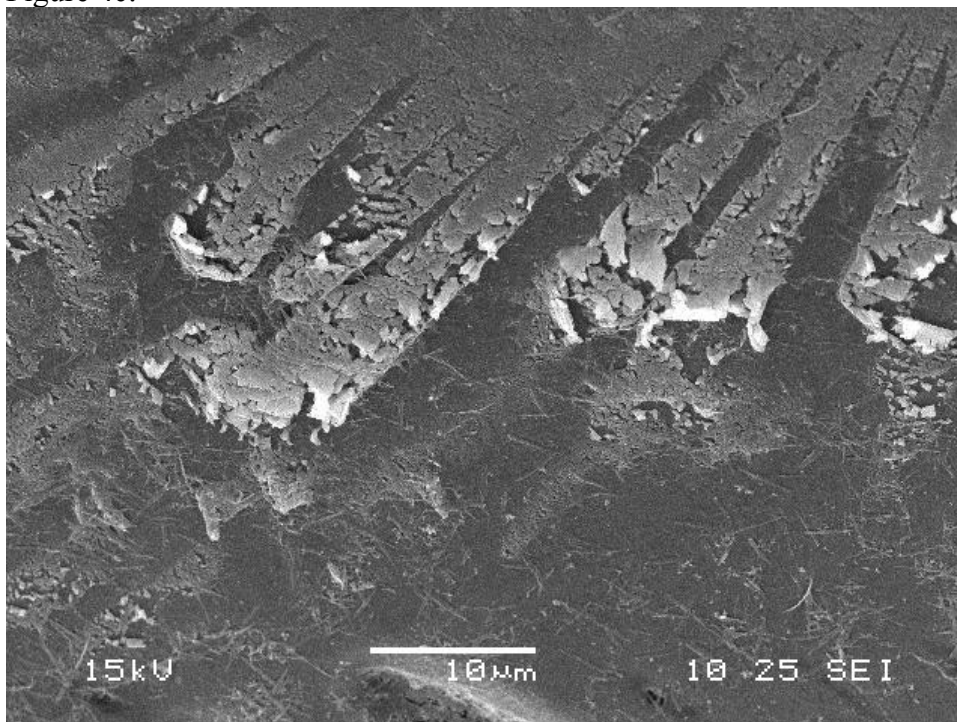


Figure 4d:

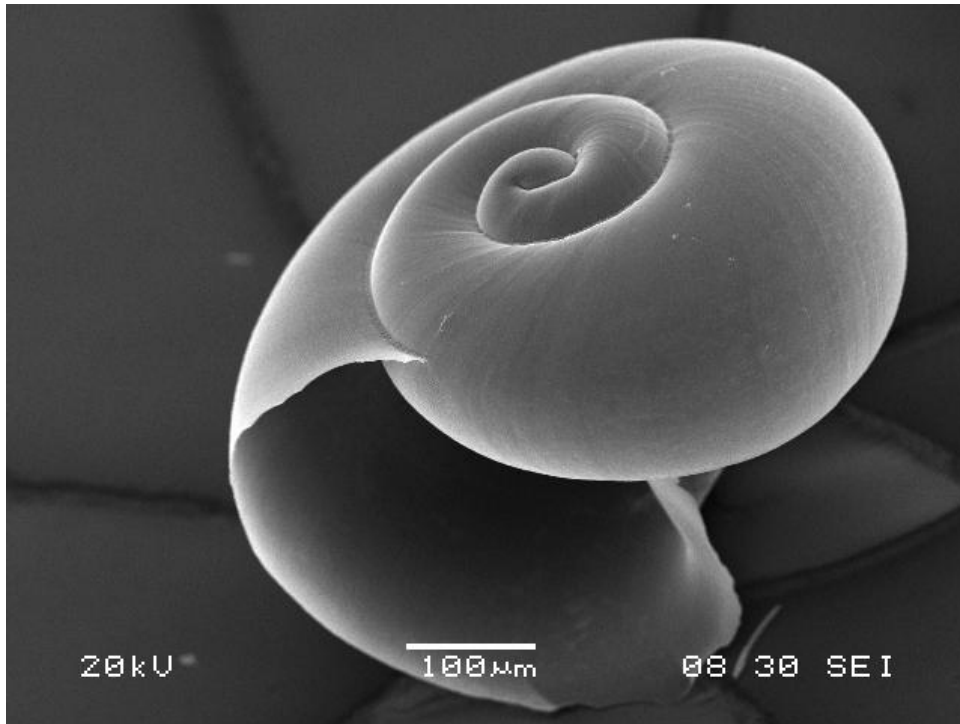


Figure 4e:

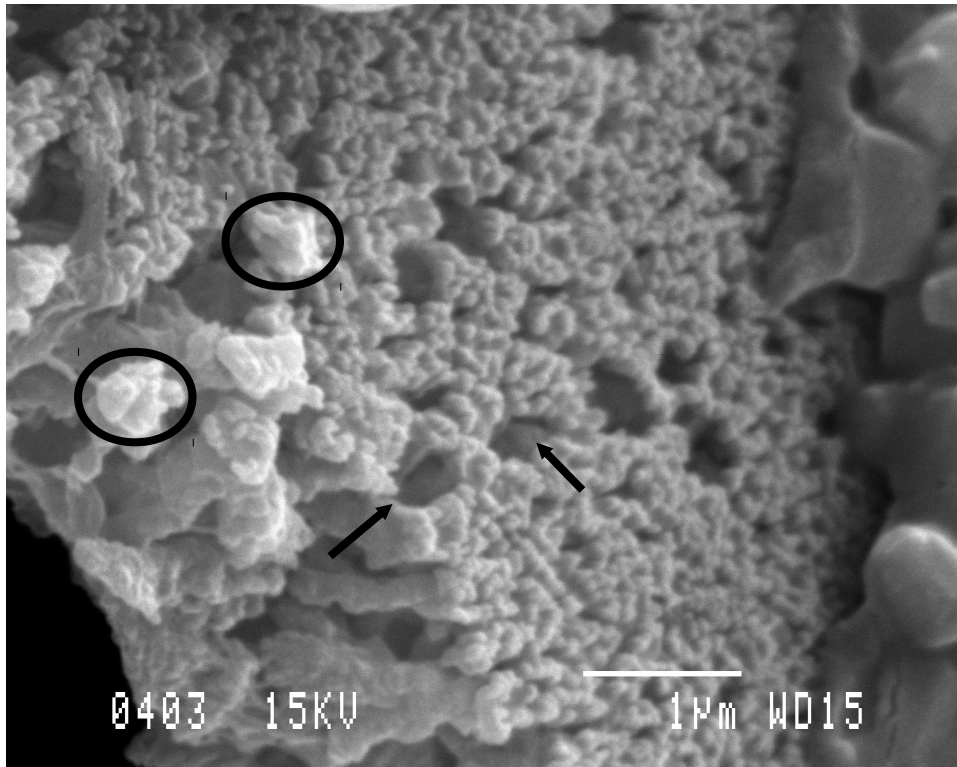


Figure 5a:

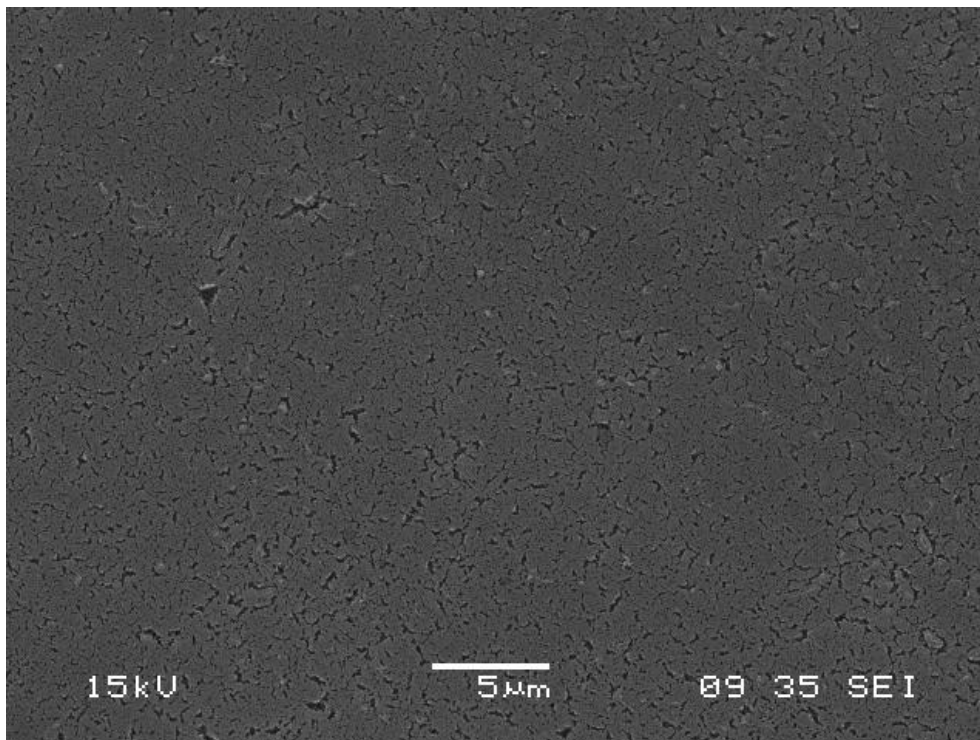


Figure 5b:

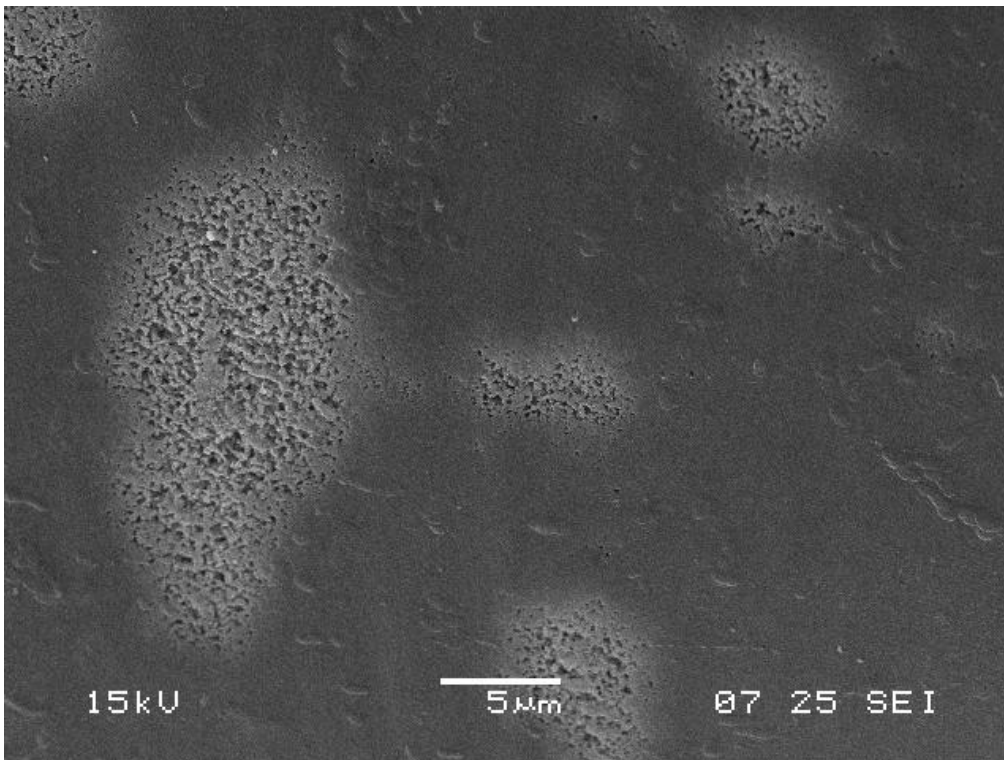


Figure 6a:

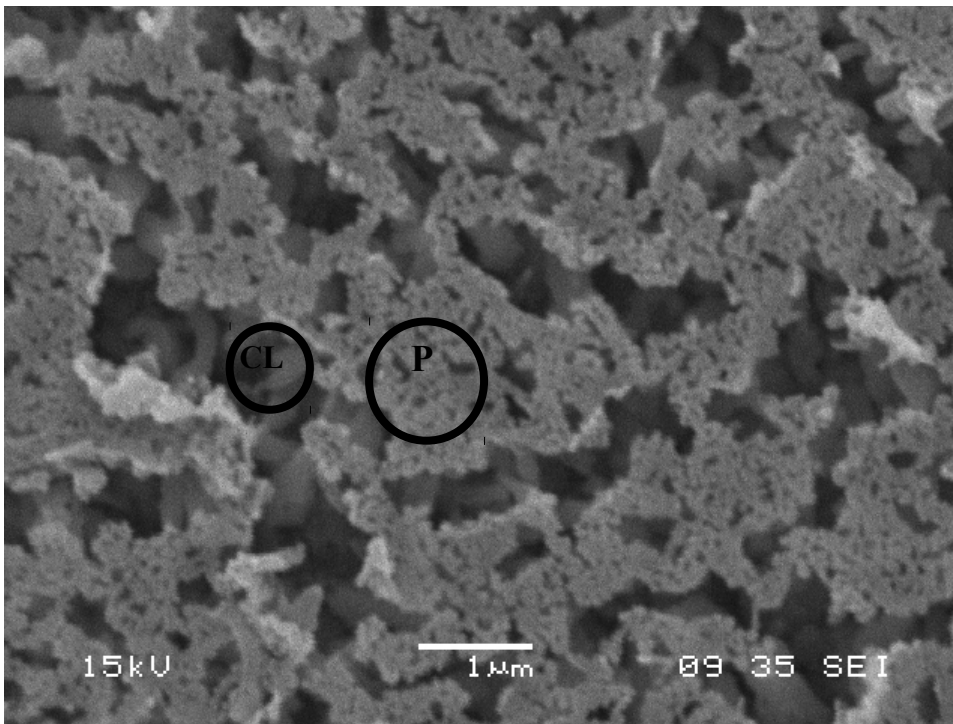


Figure 6b:

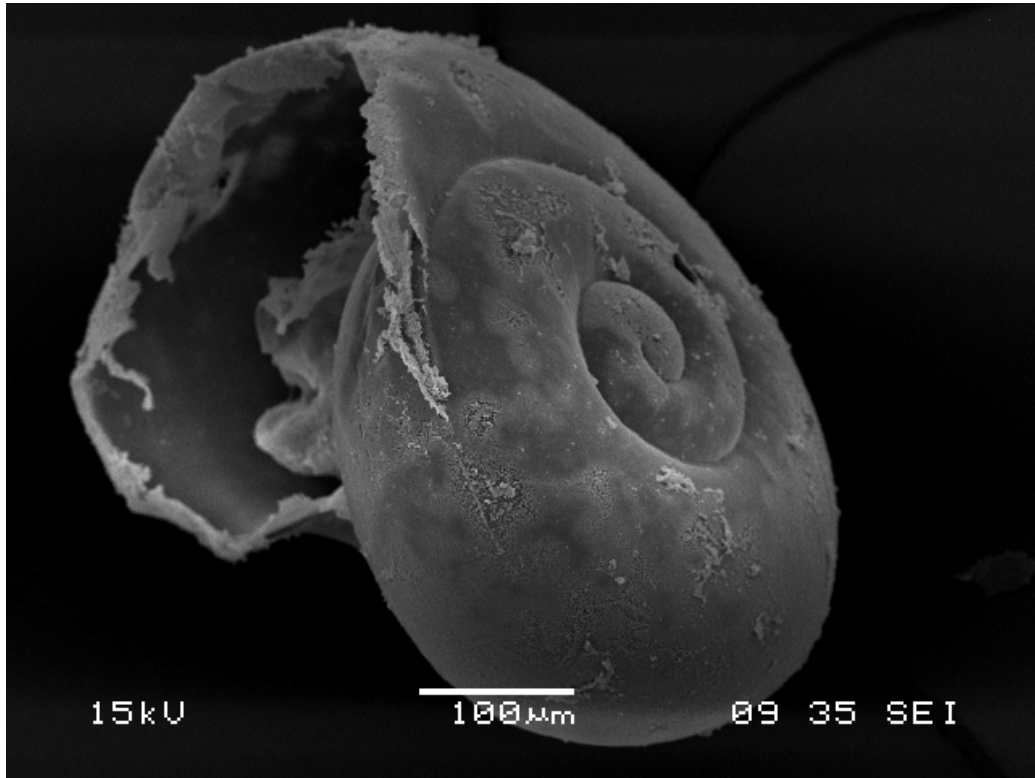


Figure 7a:

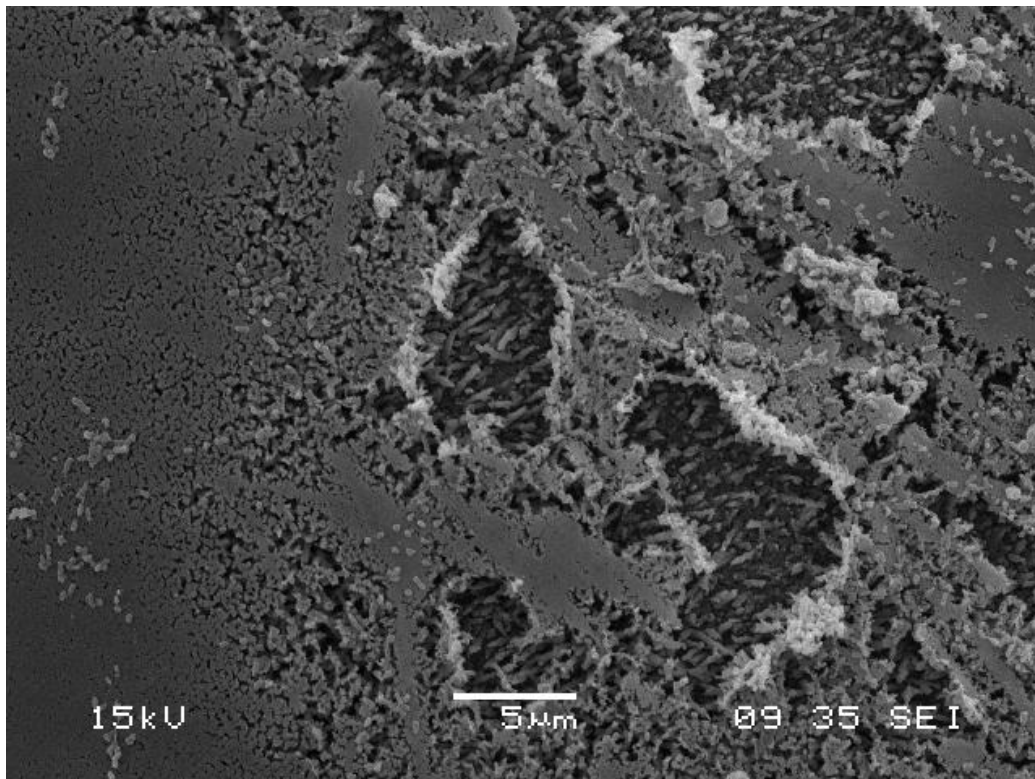


Figure 7b:

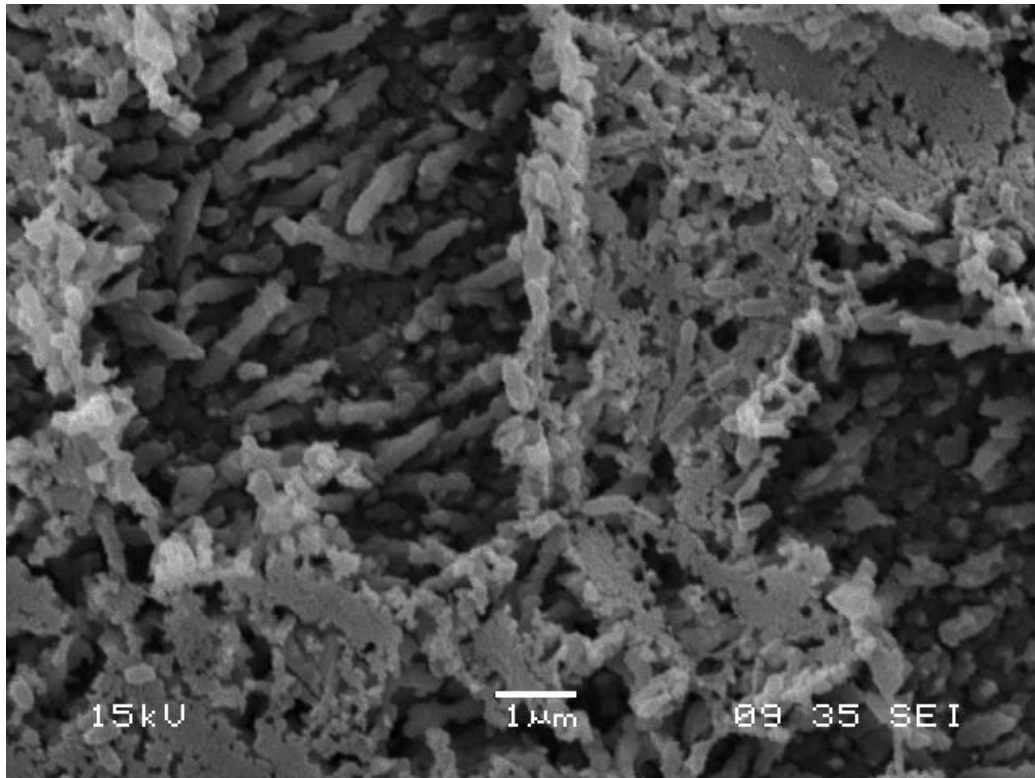


Figure 7c:

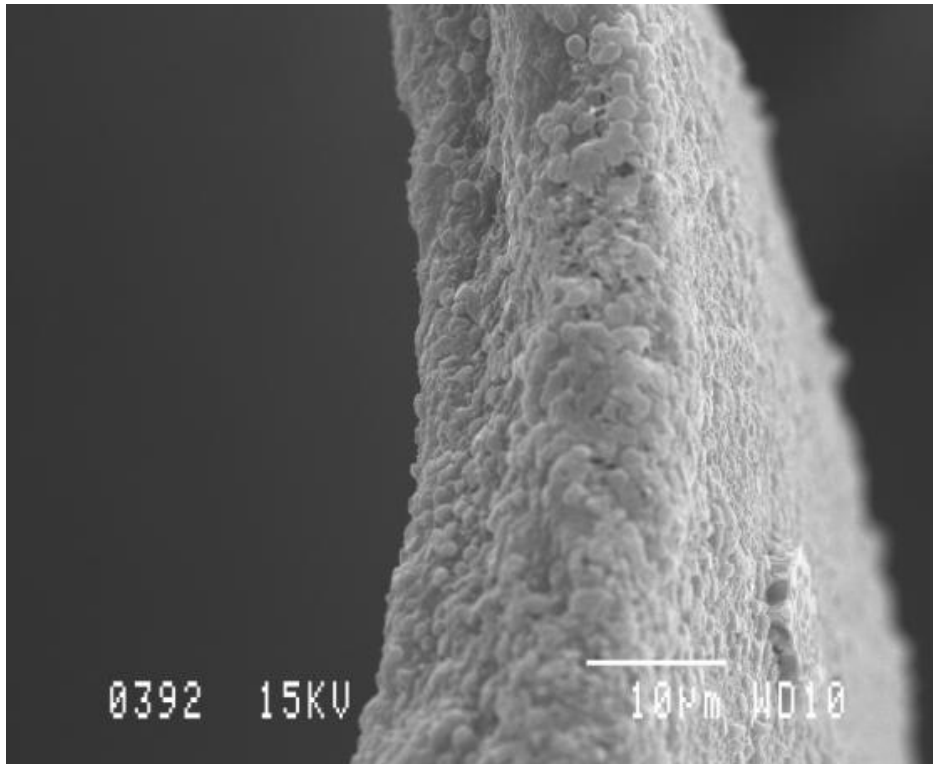


Figure 8a:

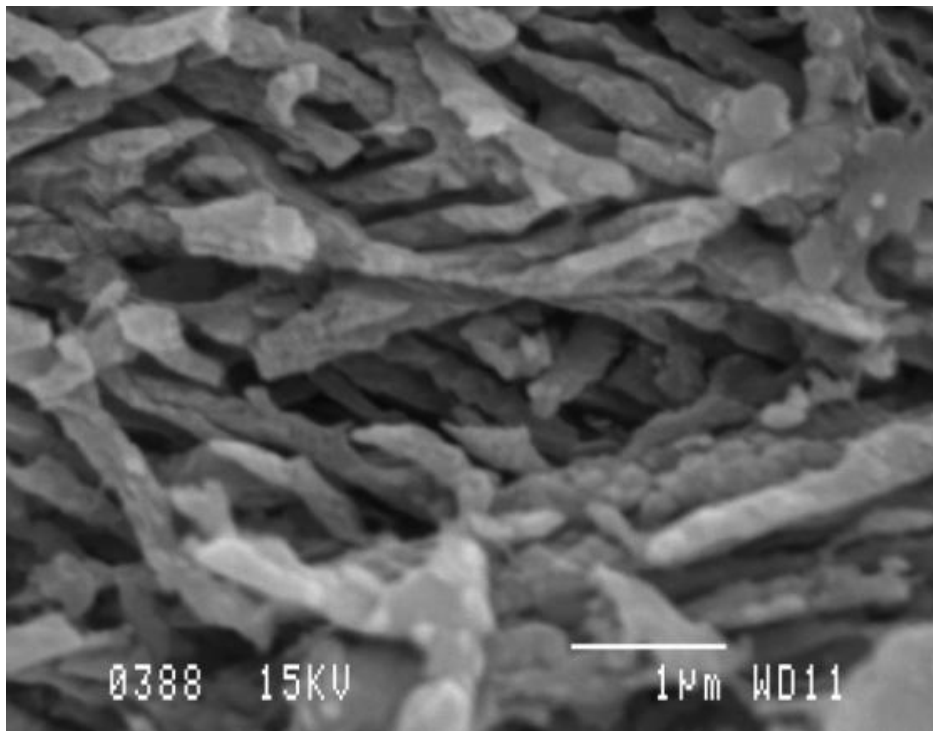


Figure 8b:

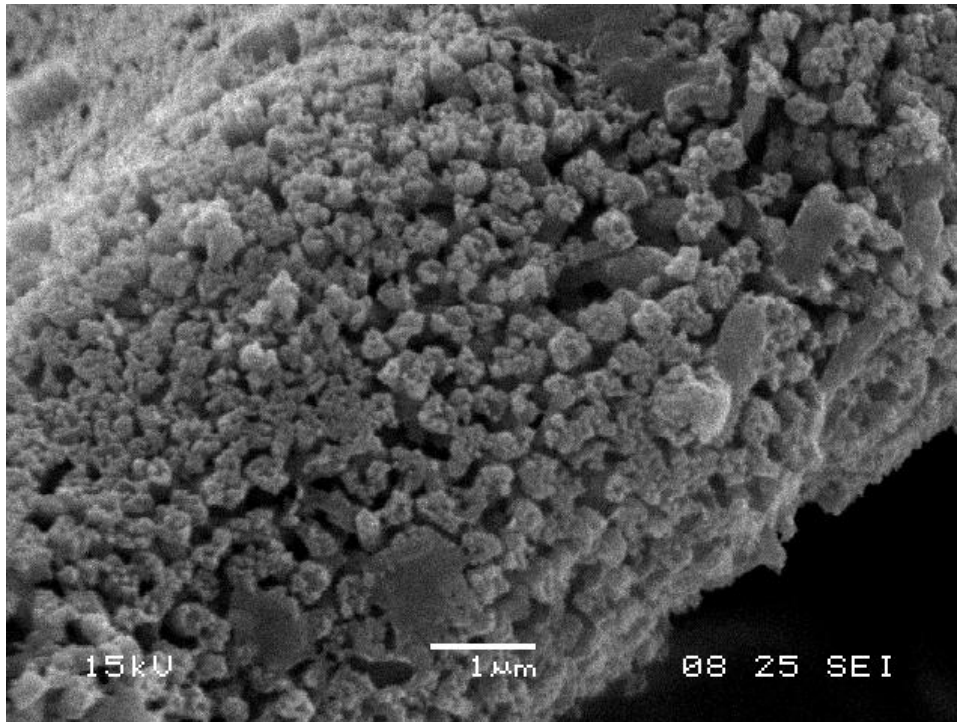


Figure 8c:

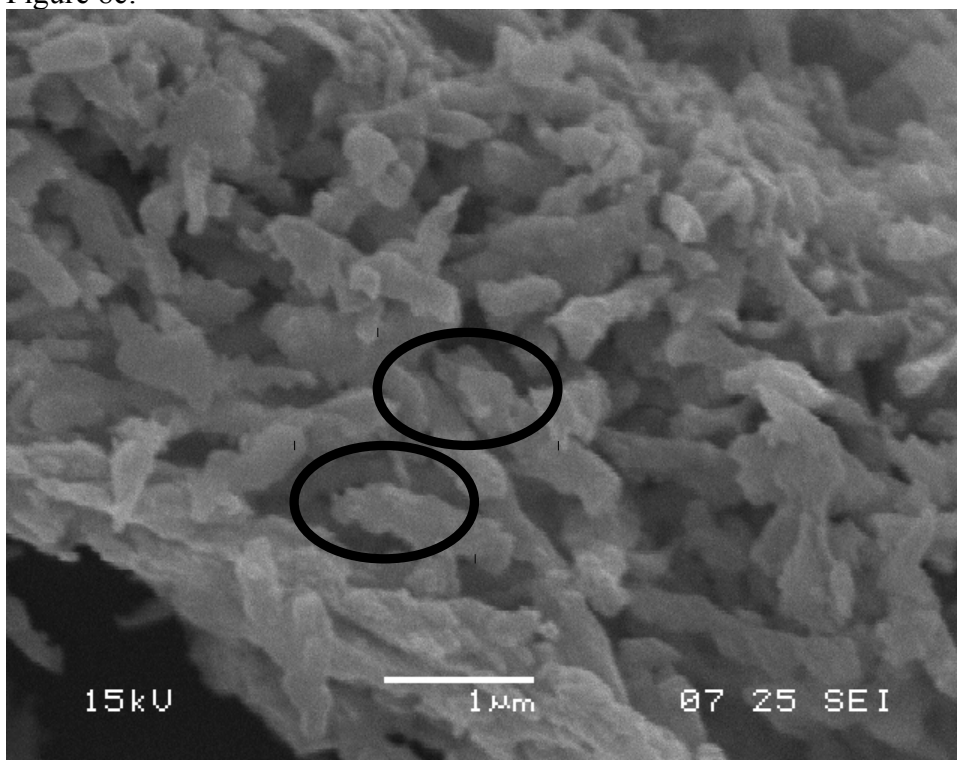


Figure 8d:

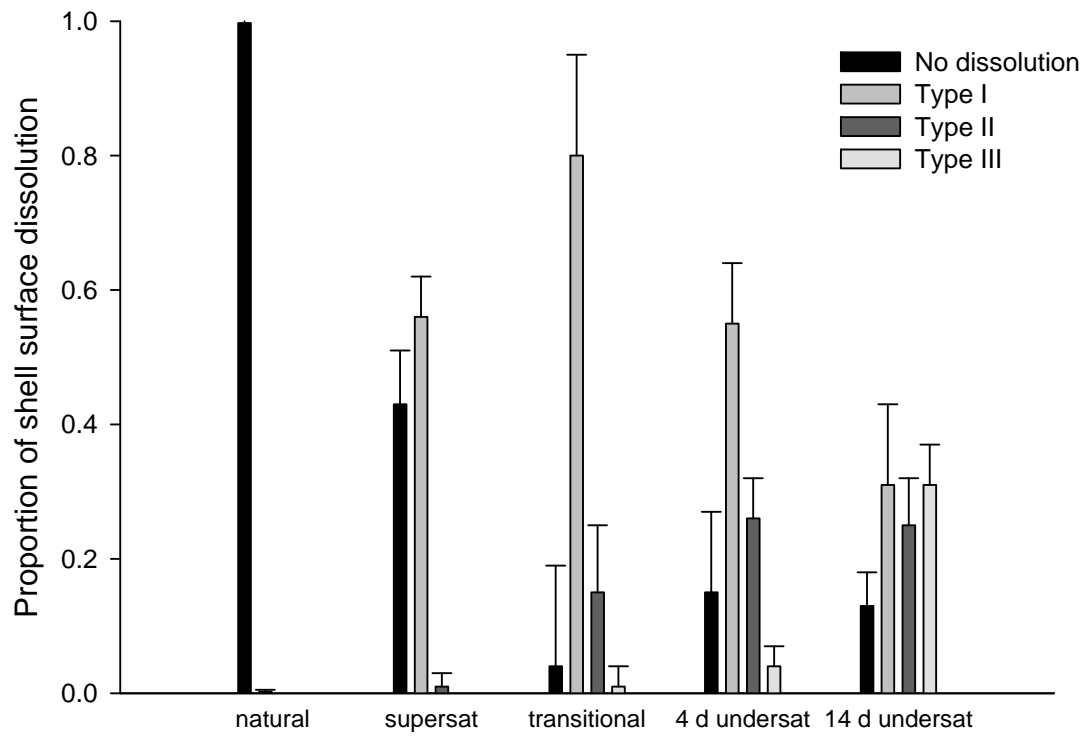


Figure 9